

(Invited Paper)

ALL-OPTICAL WAVELENGTH CONVERSION BASED ON FOUR-WAVE MIXING IN SILICON WAVEGUIDES

Shiming Gao*, Zhiqiang Li, Yanqiao Xie, Qiang Liu, Xingzhi Zhang, Yaocheng Shi, and Sailing He

Centre for Optical Electromagnetic Research, State Key Laboratory of Modern Optical Instrumentation, Zhejiang University, Hangzhou 310058, China

En-Kuang Tien and Ozdal Boyraz

Advanced Photonics Device and System Laboratory, Department of Electrical Engineering and Computer Science, University of California, Irvine, Irvine, CA 92697, USA

*gaosm@zju.edu.cn

Keywords: Wavelength conversion; four-wave mixing; silicon waveguide.

Abstract

All-optical wavelength conversion is investigated using four-wave mixing in silicon waveguides. The influences of nonlinear losses caused by two-photon absorption (TPA) and TPA-induced free-carrier absorption on the conversion efficiency and phase-matching condition are analyzed. The conversion bandwidth is tempted to enhance by optimizing the waveguide geometry and using the two-pump regime. And finally an angled-polarization pump is used to realize the polarization-independent wavelength conversion by eliminating the polarization discrepancy between the TE and TM modes.

1 Introduction

In recent years, nonlinear silicon photonics has been considered as a promising solution for the high-density integrated signal processing components in next generation optical communication systems due to the excellent integrated performance and the high nonlinear Kerr coefficient of silicon [1]. Silicon waveguides based on silicon-on-insulator (SOI) technique have exhibited the strong light confinement due to their high refractive-index contrast to improve the power intensity. Nowadays, silicon waveguides have been regarded as a new nonlinear medium for nonlinear signal processing besides quasi-phase-matching crystals, semiconductor optical amplifiers, and highly nonlinear fibers. Many kinds of nonlinear effects, such as self-phase modulation, cross-phase modulation, stimulated Raman scattering, two-photon absorption (TPA), and four-wave mixing (FWM), have been observed in silicon waveguides, and have been used to realize silicon Raman lasers, Raman amplifiers, all-optical switches, logical gates, parametric amplifiers, and wavelength converters.

In particular, wavelength conversion is an essential operation in wavelength-routing wavelength division multiplexing networks [2] and FWM in silicon waveguides has been regarded as a promising choice due to the all-optical and strict transparent characteristics, etc. Wavelength conversion has been realized in silicon waveguides using coherent anti-Stokes Raman scattering [3] or nonresonant electronic response FWM [4]-[8]. For a real-life wavelength converter, conversion efficiency and bandwidth are two important figures of merit. In addition, polarization dependency will also influence the performance of wavelength converters. In silicon waveguides, the nonlinear losses due to TPA and TPA-induced free-carrier absorption (FCA) will greatly affect the conversion efficiency [9], especially where the FCA effect is quadratically proportional to the incident power. In this paper, we will theoretically and experimentally investigate the wavelength conversion based on FWM in silicon waveguides by considering all of these lossy situations. The dispersion profile of the silicon waveguide is optimized by changing the waveguide geometry to realize broadband wavelength conversion. The conversion efficiency versus the pump power and the waveguide length is analyzed and the optimized efficiency is achieved. The bandwidth enhancement method using two-pump FWM is proposed and demonstrated experimentally. Also, the polarization-independent regime is presented to eliminate the influence of the polarization of the input signal wave.

2 Theoretical analysis

Degenerate FWM efficiently occurs when a pump wave λ_p is injected into a silicon waveguide together with a signal wave λ_s when the phase-matching condition is well satisfied. A converted wave λ_c is generated under the energy conservation condition $1/\lambda_c = 2/\lambda_p - 1/\lambda_s$. By taking into account the linear propagation loss, TPA, and FCA, the coupled equations for the FWM process under the continuous wave or quasi-continuous wave assumption can be expressed as [5]

$$\frac{dA_p}{dz} = -\frac{1}{2}(\alpha_p + \alpha_{TPAp} + \alpha_{FCAp})A_p + j\gamma_p \left[|A_p|^2 + 2|A_s|^2 + 2|A_c|^2 \right] A_p + 2j\gamma_p A_p^* A_s A_c \exp(j\Delta\beta z) \quad (1)$$

$$\frac{dA_s}{dz} = -\frac{1}{2}(\alpha_s + \alpha_{TPAs} + \alpha_{FCA_s})A_s + j\gamma_s \left[2|A_p|^2 + |A_s|^2 + 2|A_c|^2 \right] A_s + j\gamma_s A_c^* A_p^2 \exp(-j\Delta\beta z) \quad (2)$$

$$\frac{dA_c}{dz} = -\frac{1}{2}(\alpha_c + \alpha_{TPAc} + \alpha_{FCAc})A_c + j\gamma_c \left[2|A_p|^2 + 2|A_s|^2 + |A_c|^2 \right] A_c + j\gamma_c A_s^* A_p^2 \exp(-j\Delta\beta z) \quad (3)$$

where $A_{p,s,c}(z)$ are the amplitudes of the pump, the signal, and the converted waves, $\gamma_{p,s,c}$ are the nonlinear coefficients, $\Delta\beta$ is the linear phase mismatch, $\alpha_{p,s,c}$ are the linear-loss coefficients, $\alpha_{TPAp,s,c}$ and $\alpha_{FCAp,s,c}$ are the nonlinear-loss coefficients caused by the TPA and FCA effects. Mathematically the loss coefficients induced by TPA and FCA can be expressed as

$$\alpha_{TPAi} = \frac{\beta_{TPA}}{A_{eff}} \left(|A_i|^2 + 2 \sum_{m \neq i} |A_m|^2 \right), \quad (i, m = p, s, c) \quad (4)$$

$$\alpha_{FCAi} = \frac{\sigma_i \beta_{TPA} \tau}{2hcA_{eff}^2} \left(\sum_m \lambda_m |A_m|^4 + 4 \sum_{m \neq n} \frac{\lambda_m \lambda_n |A_m|^2 |A_n|^2}{\lambda_m + \lambda_n} \right), \quad (i, m, n = p, s, c) \quad (5)$$

where $\sigma_{p,s,c}$ are the FCA cross sections.

Denoting the nonlinear index coefficient of silicon as n_2 , the nonlinear coefficients for the involved waves can be calculated as

$$\gamma_i = 2\pi n_2 / \lambda_i A_{eff}, \quad (i = p, s, c) \quad (6)$$

Since all the involved waves are in the same wavelength region, it is reasonable to consider $\alpha_{p,s,c} = \alpha$, $\sigma_{p,s,c} = \sigma$, and $\gamma_{p,s,c} = \gamma$. Supposing $P_{p,s,c} = |A_{p,s,c}|^2$ the phase mismatch can be reduced to a simple expression:

$$\kappa = \Delta\beta + 2\gamma P_p = \beta_s + \beta_c - 2\beta_p + 2\gamma P_p \quad (7)$$

where $\beta_{p,s,c}$ are the wave numbers of the interacting waves.

Under lossy cases and saturation regimes only numerical solutions are available for the coupled equations (1)-(3). In particular the solution to (3) leads to the definition of the conversion efficiency and the conversion bandwidth. The calculation of conversion efficiency, which is defined as $\eta(dB) = 10 \log_{10} [P_c(z) / P_s(0)]$ provides an easy solution to the determination of the conversion bandwidth after solving (1)-(3) numerically.

3 Dispersion optimization for broadband wavelength conversion

The dispersion profile of the silicon channel waveguide is directly determined by the waveguide geometry. By selecting suitable waveguide height and width, the zero-dispersion wavelength (ZDW) can be shifted to the 1550-nm region and the dispersion can be flattened [5]. Figure 1 shows the dispersion versus the wavelength for some waveguides whose ZDWs are all around 1555 nm. For the TE mode, the dispersion slope increases as the waveguide height increases. The situation is reversed for the TM mode. The flatter the

curve is, the broader the conversion bandwidth is since the phase mismatch of the involved waves maintains small values within a wide wavelength range. After comparing the dispersion slopes of these waveguides, the waveguide cross section is optimized as $400 \times 269 \text{ nm}^2$ for the TM mode in order to obtain the smallest dispersion slope that corresponds to the broadest conversion bandwidth.

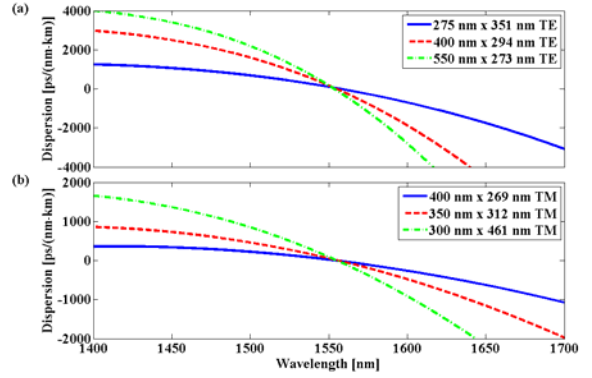


Figure 1: Dispersion as a function of the wavelength for (a) TE and (b) TM modes.

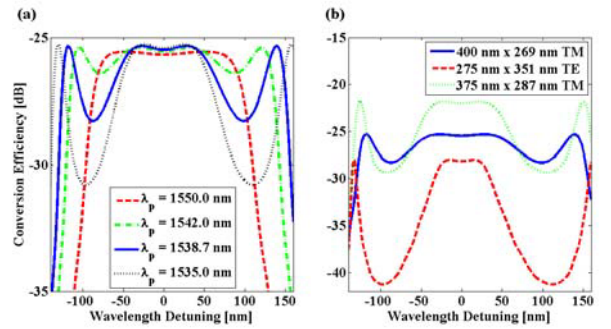


Figure 2: (a) Conversion efficiency versus the wavelength detuning for different pump wavelengths in the optimized $400 \times 269 \text{ nm}^2$ waveguide; (b) Conversion response comparison of the $400 \times 269 \text{ nm}^2$, $275 \times 351 \text{ nm}^2$, and $375 \times 287 \text{ nm}^2$ waveguides with the optimized pump wavelength.

Figure 2(a) shows the conversion efficiency versus the wavelength detuning for different pump wavelengths in the anomalous region in the optimized waveguide of $400 \times 269 \text{ nm}^2$ with a fixed input power of 200 mW, $\alpha = 2.5 \text{ dB/cm}$, $\sigma = 1.45 \times 10^{-17} \text{ cm}^2$, $\beta_{TPA} = 0.3 \text{ cm/GW}$, and $\tau = 1 \text{ ns}$. When the pump is tuned away from the ZDW, the appearance of a second pair of conversion efficiency peaks farther from the pump, which is introduced by the location shift and number increase of the perfect phase-matched wavelengths, increase the 3-dB bandwidth. The maximum conversion bandwidth is achieved when pumping at 1538.7 nm under the assumption of 200-mW input pump power and 2-cm-long interaction length. Figure 2(b) simulates the conversion response for the optimized $400 \times 269 \text{ nm}^2$ waveguide for TM polarization together with two other waveguides with the dimensions of $275 \times 351 \text{ nm}^2$ for TE polarization and $375 \times 287 \text{ nm}^2$ for TM polarization. These results are obtained in a 2-cm-long waveguide with a 200-mW pump wave at 1538.7 nm. The 3-dB bandwidth is over 280 nm for the optimized waveguide

and the bandwidths of $275 \times 351 \text{ nm}^2$ and $375 \times 287 \text{ nm}^2$ waveguides are 77 nm and 112 nm.

4 Influence of waveguide length and pump power

The FWM efficiency in silicon waveguides will be greatly affected by the nonlinear losses due to TPA and TPA-induced FCA, which is dominated by the incident power. In such a situation, higher pump power and longer waveguide cannot ensure the increase of conversion efficiency [6].

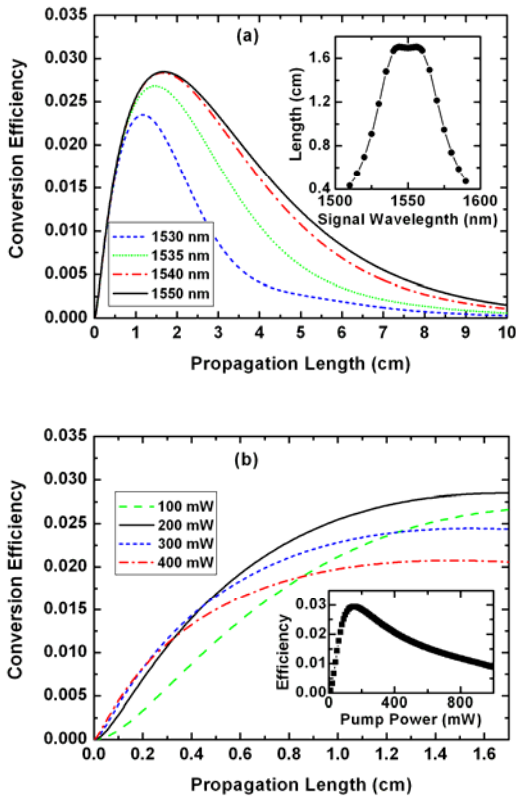


Figure 3: (a) Conversion efficiency for different signal wavelengths and the inset shows the optimized waveguide length versus the signal wavelength; (b) conversion efficiency evolution in a 1.7-cm-long waveguide for different incident pump powers, and the inset shows the output efficiency versus the incident pump power.

In a $300 \times 500 \text{ nm}^2$ silicon waveguide, by considering $\alpha = 1.95 \text{ dB/cm}$, $\beta_{TPA} = 0.5 \text{ cm/GW}$, $\sigma = 1.45 \times 10^{-17} \text{ cm}^2$, $\tau = 3.5 \text{ ns}$, and $A_{eff} = 9.484 \times 10^{-2} \text{ } \mu\text{m}^2$, the conversion efficiency along the waveguide is simulated for several different signal wavelengths, as shown in Fig. 3(a), where the pump is fixed as 200 mW at the wavelength of 1550 nm. For every signal wavelength, the propagation distance for the maximum efficiency is much shorter than the coherent length. Over this distance, the received energy is not enough to compensate the loss- and absorption-induced attenuations any more and the efficiency declines gradually, although the energy is still converted from the pump to the converted wave. As shown in the inset of Fig. 3(a), the optimized waveguide lengths for the

signals around the pump within a region of about 20 nm are almost the same (1.7 cm). It is reasonable to consider 1.7 cm as the optimal length.

Considering a 1.7-cm-long waveguide, the conversion efficiencies along the waveguide for several incident pump powers are simulated in Fig. 3(b). The efficiency peak of the 200-mW pump just locates at the end of the waveguide. If a much higher pump power such as 300 or 400 mW is used, the output efficiency will obviously drop and lower than the 100-mW case due to absorptions. The output efficiency is shown in the inset of Fig. 3(b) according to the pump power.

Figure 4 shows the conversion efficiency and bandwidths in terms of the pump power and waveguide length. In Fig. 4(a), the global maximum efficiency is achieved with the optimized pump of 152 mW in a 1.79-cm-long waveguide. In Fig. 4(b), the conversion bandwidth rapidly decreases with the waveguide length increasing. The bandwidth corresponds to the maximum efficiency is 47 nm, which is enough to cover the entire C-band.

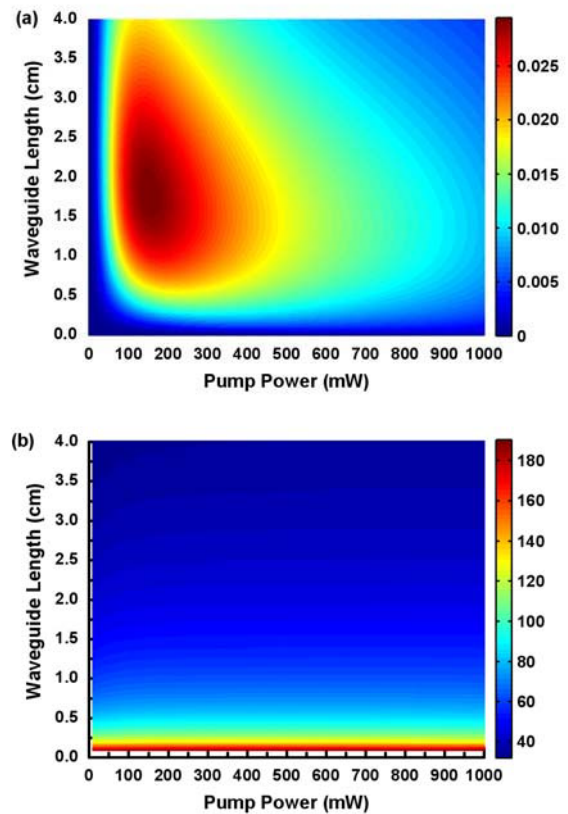


Figure 4: (a) Conversion efficiency and (b) bandwidth distributions versus the pump power and the waveguide length.

5 Bandwidth enhancement using two-pump FWM

Analysis has shown that the phase-matching condition of FWM can be freely controlled by the pump spacing when two-pump regime is used [7]. Considering a 1.5-cm-long $300 \times 500 \text{ nm}^2$ waveguide that corresponds to $9.838 \times 10^{-2} \text{ } \mu\text{m}^2$ effective mode area, $\alpha = 2.5 \text{ dB/cm}$, $\beta_{TPA} = 0.5 \text{ cm/GW}$ for

degenerate/nondegenerate absorption, $\sigma = 1.45 \times 10^{-17} \text{ cm}^2$, and $\tau = 2 \text{ ns}$. The phase mismatches of the degenerate FWM with a single pump are shown in Figs. 5(a) and 5(b) corresponding to the pump powers of 100 and 1000 mW respectively when the pump wavelength is 1550 nm. Although the incident pump power is dramatically increased, the phase mismatch varies slightly due to TPA and FCA, especially after the 0.5-cm-long transmission. As a result, their bandwidths are 53.0 and 58.1 nm for the two cases and only have a 5.1-nm difference, as shown in Fig. 6(a). However, the phase mismatch can be greatly changed by setting the pump wavelengths in the nondegenerate scheme with two pumps because the phase-matched condition is dominated by the wave numbers of the involved waves. Figures 5(c) and 5(d) show the phase mismatches for the 10- and 43.16-nm pump spacing, where the mean pump wavelength is fixed at 1550 nm. It is shown that the two perfect phase-matched curves go away from each other when the two pumps are set apart. A visual effect shown in the corresponding responses in Fig. 6(b) is the enhancement of bandwidth. The bandwidths are read to be 53.5 and 67.8 nm for the two pump wavelength spacings. It is 14.8 nm (28%) enhanced compared with the degenerate scheme under the same level of pump power.

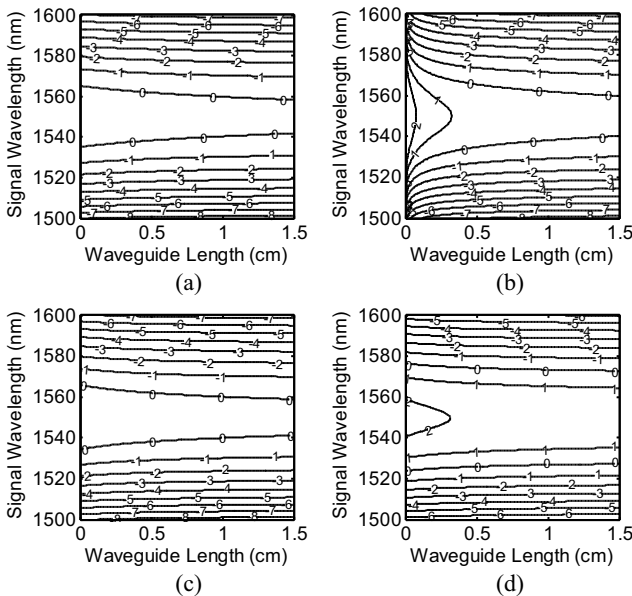


Figure 5: Phase mismatches of the single-pump FWM for (a) 100-mW and (b) 1000-mW pumps and of the two-pump FWM for (c) 10-nm and (d) 43.16-nm pump spacings.

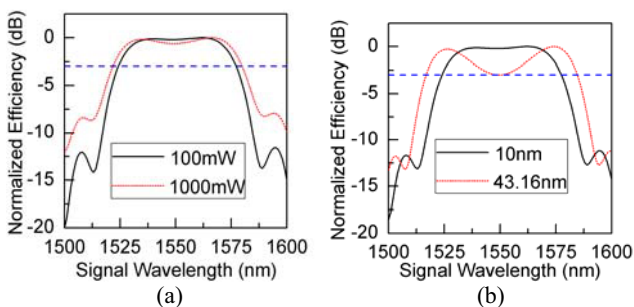


Figure 6: Conversion responses for (a) the single-pump FWM and (b) the two-pump FWM.

As shown in Fig. 6(b), the nonuniformity of the conversion response is also concomitantly enhanced with the pump spacing of the nondegenerate FWM increasing since the central signals suffer from larger phase mismatch, which means lower conversion efficiency. Here one can see that the response nonuniformity reaches 3 dB for 43.16-nm wavelength spacing and the 3-dB bandwidth becomes discontinuous when the pump spacing is further increased. And then, the conversion bandwidth will decrease as the pump spacing increases, which is not beneficial to the wavelength conversion function. Therefore, the optimized 3-dB bandwidth can be obtained to be 67.8 nm in the $300 \times 500 \text{ nm}^2$ SOI waveguide we considered.

The conversion efficiency can be experimentally obtained from the measured FWM spectra, as shown in Fig. 7. It is noticeable that the efficiency is tightly related to the pump powers, i.e., $\eta_{nd} \propto P_{p1}P_{p2}$ and $\eta_d \propto P_p^2$. In the experiments, the gains in the EDFA will be difference for the two-pump and single-pump cases. For comparison, the unit conversion efficiencies are used in Fig. 7 to eliminate the influence of the pump powers (i.e. $\eta_{nd-norm} = \eta_{nd}/P_{p1}P_{p2}$ and $\eta_{d-norm} = \eta_d/P_p^2$) [4]. By fitting the experiment conversion responses, the experimental bandwidths are calculated from Fig. 7. The half bandwidth of degenerate FWM is about 14.9 nm, while it is about 18.7 nm for the degenerate FWM. The experimental results agree well with the theoretical simulation and the bandwidth enhancement is verified. Due to the limitation of the tuning range of the filter, the pump spacing can not be larger in our experiment. A broader bandwidth will be achieved if the pumps can be separated further, which has been predicted in theoretical analysis.

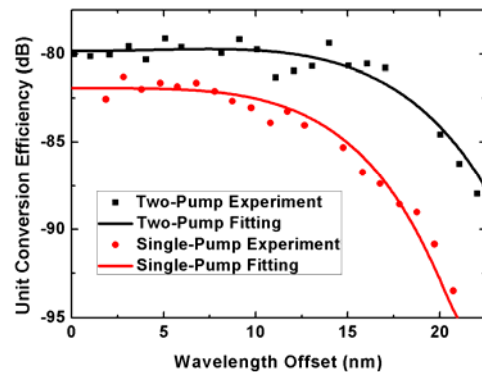


Figure 7: Measured unit conversion efficiencies and the fitting curves for the single-pump and two-pump wavelength conversions.

6 Design of polarization-independent wavelength conversion

The dispersions of the SOI channel waveguide are often different for the TE and TM modes due to the asymmetry of substrate and cladding, which causes the polarization dependency on the incident signal. Here we propose to eliminate this effect by using an angled pump [8]. The principle is shown in Fig. 8. When the pump is incident into

the waveguide with an angle, FWM effects will occur along both TE and TM modes. By optimizing the pump angle to control the FWM strengthens to make them almost the same for the TE and TM modes, the conversion efficiency will be almost a constant regardless of the incident signal polarization.

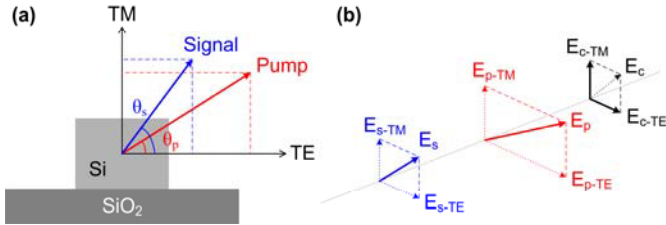


Figure 8: Principle of the polarization-independent wavelength conversion with an angled-polarization pump in a silicon waveguide.

Considering a $285 \times 650 \text{ nm}^2$ waveguide, the coupling efficiency ratio of the TE to TM mode is calculated to be $C_{TE}/C_{TM} = 0.356$ through mode filed overlapping integral method. The simulation parameters are considered as follows: $A_{eff-TE} = 0.1180 \mu\text{m}^2$, $A_{eff-TM} = 0.1178 \mu\text{m}^2$, $\alpha_{Lin-TE} = 2.5 \text{ dB/cm}$, $\alpha_{Lin-TM} = 2 \text{ dB/cm}$, $\beta_{TPA} = 0.5 \text{ cm/GW}$, $\sigma = 1.45 \times 10^{-17} \text{ cm}^2$, $\tau = 2.5 \text{ ns}$. Here the waveguide length is assumed to be $L = 0.8 \text{ cm}$. The required pump angle is related to the losses and the phase mismatches of the TE and TM modes. Since the phase mismatch varies with the signal wavelength, the required pump polarization angle also changes for different signal waves. Fortunately, the fluctuation of the pump angle for each signal wavelength is very slight when the signal and the pump are in the same wavelength region. Assuming the incident pump power is 100 mW at wavelength 1550 nm, the required pump polarization angle is calculated to be 23.784° .

Using the determined pump angle, the generated converted signal power and the corresponding conversion efficiency are calculated by assuming the signal power as 1 mW. The conversion efficiency is calculated for several typical signal wavelengths with arbitrary incident polarization angles, as shown in Fig. 9(a), where the signal angle is considered in the range from 0 to 90° since this is enough to represent all kinds of FWM between the pump and signal. Their conversion efficiencies are a bit different from each other because of the different phase mismatch values. In Fig. 9(a), the conversion efficiency for each signal wavelength varies very slightly with the signal polarization angle. Since the optimized pump angle gives priority to the signals near the pump to ensure their polarization insensitivity, the efficiency fluctuations become large for signals far from the pump. For example, the efficiency fluctuations are 0.007 dB for the 1550- and 1560-nm signal, and it is 0.093 dB for the 1570-nm signal. The efficiency fluctuation increases to 0.686 dB when the signal wavelength reaches 1580 nm, which is 30-nm away from the pump.

Figure 9(b) illustrates the conversion efficiency versus the signal wavelength corresponding to Fig. 9(a). Here the maximum and the minimum efficiencies are used to show the conversion efficiency fluctuation when freely changing the incident signal polarization. In Fig. 9(b), one sees that the 1-dB polarization-insensitive bandwidth is 64 nm and the

efficiency fluctuation is less than 0.013 dB for the signals in the 30-nm range around the 1550-nm pump. The wavelength conversion scheme we presented exhibits excellent polarization-insensitive characteristic in the entire C-band.

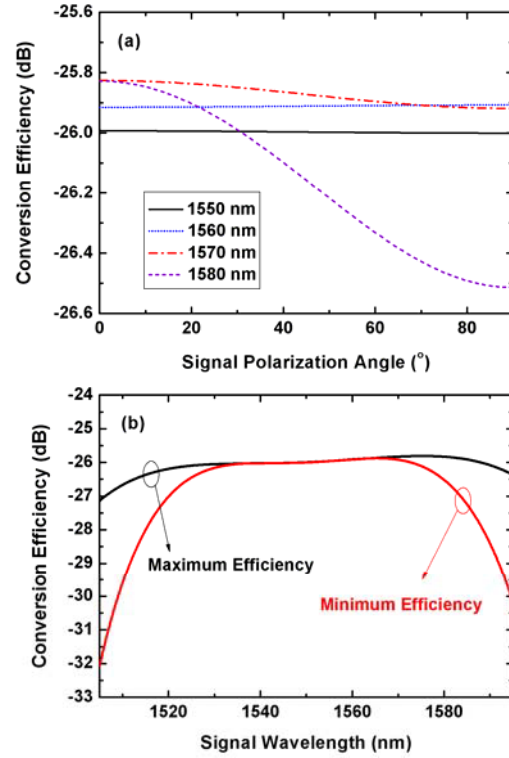


Figure 9: (a) Conversion efficiencies versus the incident signal polarization angle for several signal wavelengths; (b) Maximum and minimum conversion efficiencies versus the signal wavelength.

6 Conclusion

We have investigated the wavelength conversion based on FWM in silicon waveguides. The influence of TPA and FCA on the phase matching and efficiency has been studied. The bandwidth enhancement has been realized by engineering the dispersion through the waveguide geometry optimization and using two-pump FWM. A method for polarization-independent wavelength conversion with an angled pump has been proposed and numerically demonstrated.

Acknowledgements

This work was supported by the National Natural Science Foundation of China (Grant Nos. 60708006, 60978026, and 60688401), the Specialized Research Fund for the Doctoral Program of Higher Education of China (Grant No. 20070335118), and the Zhejiang Provincial Natural Science Foundation of China (Grant No. Y1090379).

References

- [1] R. Dekker, N. Usechak, M. Först, and A. Driessen, "Ultrafast nonlinear all-optical processes in silicon-on-

- insulator waveguides,” *J. Phys. D-Appl. Phys.*, **vol. 40**, pp. R249-R271, (2007).
- [2] S. J. B. Yoo, “Wavelength conversion technologies for WDM network applications,” *J. Lightwave Technol.*, **vol. 14**, pp. 955-966, (1996).
- [3] V. Raghunathan, R. Claps, D. Dimitropoulos, and B. Jalali, “Parametric Raman wavelength conversion in scaled silicon waveguides,” *J. Lightwave Technol.*, **vol. 23**, pp. 2094-2102, (2005).
- [4] S. Gao, E.-K. Tien, Q. Song, Y. Huang, and O. Boyraz, “Ultra-broadband one-to-two wavelength conversion using low-phase-mismatching four-wave mixing in silicon waveguides,” *Opt. Express*, **vol. 18**, pp. 11898-11903, (2010).
- [5] X. Zhang, S. Gao, and S. He, “Optimal design of a silicon-on-insulator nanowire waveguide for broadband wavelength conversion,” *Prog. Electromagn. Res.*, **vol. 89**, pp. 183-198, (2009).
- [6] S. Gao, Z. Li, and X. Zhang, “Power-attenuated optimization for four-wave mixing-based wavelength conversion in silicon nanowire waveguides,” *J. Electromagn. Waves Appl.*, **vol. 24**, pp. 1255-1265, (2010).
- [7] S. Gao, Z. Li, E.-K. Tien, Q. Liu, S. He, and O. Boyraz, “Broadband wavelength conversion by nondegenerate four-wave mixing in a silicon-on-insulator waveguide,” in *Tech. Dig., Integr. Photon. Res. Conf.*, Monterey, CA, 2010, paper IWC2.
- [8] S. Gao, X. Zhang, Z. Li, and S. He, “Polarization-independent wavelength conversion using an angled-polarization pump in a silicon nanowire waveguide,” *IEEE J. Sel. Top. Quantum Electron.*, **vol. 16**, pp. 250-256, (2010).
- [9] X. Sang and O. Boyraz, “Gain and noise characteristics of high-bit-rate silicon parametric amplifiers,” *Opt. Express*, **vol. 16**, pp. 13122-13132, (2008).